J Nanostruct 16(3): 3039-3052, Summer 2026

RESEARCH PAPER

Sustainable and Green Bio-Preparation of Selenium Nanoparticles and Their Antibacterial and Photocatalytic Activity

Asokan Vasudevan [1]*, Sanan Thaer Abdalwahab [2], Zainab Malik Salem [3], Suad Abdulnaser [4], Mohannad Abdulrazzaq Gati [5], Jabar Juad [6], Suleiman Ibrahim Mohammad [7], Oripov Firdavs [8], Saidov Akbar [9], Khalilzade Eldar [9], Babaev Khamza [10], Murodiljon Boltaboyev [11], Bahodirjon Davlatov [12], Kaxarov Abdukaxor [13]

[1] *Faculty of Business and Communications, INTI International University, 71800 Negeri Sembilan, Malaysia*

[2] *Department of Pharmacy, Al-Turath University, Baghdad, Iraq*

[3] *Department of Pharmacy, College of Pharmacy, Al-Nisour University, Baghdad, Iraq*

[4] *Al-Hadi University College, Baghdad, Iraq*

[5] *College of Health and Medical Technologies, National University of Science and Technology, Dhi Qar, Iraq*

[6] *Al-Zahrawi University, Karbala, Iraq*

[7] *INTI International University, 71800 Negeri Sembilan, Malaysia*

[8] *Department of Histology, Samarkand State Medical University, Samarkand, Uzbekistan*

[9] *Department of Orthopedic Dentistry and Orthodontics, Bukhara State Medical Institute, Bukhara, Uzbekistan*

[10] *Department of Pathological Anatomy, Tashkent State Medical University, Tashkent, Republic of Uzbekistan*

[11] *Department of Epidemiology and Infectious Diseases, Nursing, Fergana Medical Institute of Public Health, Fergana, Uzbekistan*

[12] *Tashkent State Technical University, Tashkent, Uzbekistan*

[13] *Department of Infectious Diseases, Andijan State Medical Institute, Andijan, Uzbekistan*

ARTICLE INFO

Article History:
Received 10 March 2026
Accepted 08 May 2026
Published 01 July 2026

Keywords:
Antibacterial
Bio-synthesis
Green synthesis
Photocatalyst
Selenium nanoparticles

ABSTRACT

This study reports a facile, entirely green synthesis of selenium nanoparticles (Se NPs) using an aqueous extract of *Artemisia annua* leaves as both a reducing and stabilizing agent. The bioreduction of sodium selenite yielded quasi-spherical, crystalline nanoparticles with an average diameter of 38 ± 7 nm, as confirmed by TEM and XRD analysis. FT-IR and TGA investigations revealed the formation of a substantial phytochemical corona (15–20% by mass), comprising polyphenols and flavonoids from the extract, which is responsible for colloidal stability and surface functionality. The biosynthesized Se NPs exhibited potent, broad-spectrum antibacterial activity, demonstrating bactericidal action with minimum inhibitory concentrations (MICs) of 25 µg/mL against *Staphylococcus aureus* and 50 µg/mL against *Escherichia coli*. Furthermore, the Se NPs functioned as an efficient visible-light photocatalyst, degrading 94.7% of methylene blue within 120 minutes (rate constant *k* = 0.0221 min^{-1}) and maintaining 88.3% efficiency over three reuse cycles. The dual functionality is attributed to the synergistic interplay between the narrow-bandgap trigonal selenium core and the bioactive capping layer. This work establishes a sustainable protocol for fabricating multifunctional Se NPs with significant potential in antimicrobial applications and environmental remediation.

How to cite this article
Vasudevan A., Abdalwahab S., Salem Z. et al. Sustainable and Green Bio-Preparation of Selenium Nanoparticles and Their Antibacterial and Photocatalytic Activity. J Nanostruct, 2026; 16(3):3039-3052. DOI: 10.22052/JNS.2026.03.004

* *Corresponding Author Email: ameralnafiey@outlook.com*

INTRODUCTION

The burgeoning field of nanotechnology has placed significant emphasis on selenium nanoparticles (Se NPs) due to their intriguing biological activities, including antioxidant, anticancer, and antimicrobial properties, alongside their utility in environmental remediation as photocatalysts [1-4]. However, conventional physicochemical methods for Se NP synthesis often involve harsh reducing agents, organic solvents, and high energy inputs, raising concerns regarding environmental toxicity, cost, and scalability [5-8]. This has catalyzed a paradigm shift towards sustainable and green synthesis methodologies, which align with the principles of green chemistry by minimizing waste and leveraging benign reagents [9-14]. Historically, the exploration of biological systems for nanoparticle synthesis draws from the ancient recognition of microbial metal resistance and reduction mechanisms, but its deliberate application for nanomaterial fabrication has gained substantial momentum only in the last two decades. Contemporary green synthesis strategies predominantly utilize biological entities such as plant extracts, fungi, bacteria, and algae [15]. These systems provide a rich repertoire of phytochemicals (e.g., polyphenols, flavonoids, alkaloids) or microbial enzymes and proteins that act as both reducing agents, converting selenite or selenate salts to elemental selenium (Se^0), and capping agents, stabilizing the nascent nanoparticles and preventing aggregation [16-18]. The plant-mediated approach, in particular, has garnered extensive attention for its simplicity, rapid reaction kinetics at ambient conditions, and elimination of complex cell culture maintenance. Each biological source imparts distinct biochemical influences, allowing for nuanced control over critical Se NP characteristics such as size distribution, morphology, and surface chemistry, which are paramount for tailoring their subsequent applications [19, 20]. Therefore, the development of robust, eco-conscious bio-preparation protocols is not merely an alternative but a necessary evolution to produce functional Se NPs with lower environmental footprint, enhanced biocompatibility, and potential for large-scale industrial translation, forming a critical foundation for their advanced investigation in biomedicine and catalysis.

Recent advances in the green biosynthesis of Se NPs have focused on refining the precision, mechanistic understanding, and functionalization of these processes, moving beyond mere proof-of-concept demonstrations [21-23]. A significant trend is the strategic selection and pre-treatment of biological sources to enhance reducing efficiency and control nanoparticle properties. For instance, the use of specific plant parts (e.g., seed coats, fruit peels, or root extracts) rich in targeted polyphenolic compounds has allowed for more reproducible synthesis of Se NPs with defined sizes between 10-100 nm [24, 25]. Furthermore, research has elucidated the roles of specific biomolecules, such as glutathione in fungal systems or epigallocatechin gallate in tea extracts, in the sequential reduction and stabilization mechanisms, providing a foundational rationale for what was previously largely empirical. Another notable advancement is the integration of hybrid and assisted biosynthesis methods. Techniques like microwave-assisted extraction of plant metabolites prior to synthesis, or the use of ultrasonic irradiation during the bioreduction step, have markedly improved reaction kinetics and yield while promoting narrower size distributions [26-28]. Similarly, the exploration of agricultural and food industry by-products such as fruit pomace, spent coffee grounds, or lignocellulosic waste as cheap and abundant source materials has gained traction, aligning synthesis with circular economy principles. Concurrently, there is a growing emphasis on *in-situ* functionalization, where the capping agents inherent to the biological extract are engineered to impart immediate functionality, such as enhanced colloidal stability in physiological buffers or inherent photocatalytic activity through charge-transfer complexes. These sophisticated approaches collectively represent a maturation of the field, transitioning from simple green synthesis to the design of biologically templated, application-ready Se NP hybrids with tailored surface chemistry and improved performance metrics [23, 29]. Table 1 shows types of approach for bio-synthesis of Se NP including plant-mediated synthesis (Phyto-synthesis), microbial synthesis, marine organisms, and enzyme & biomolecule-mediated synthesis [30, 31].

Recent investigations have significantly expanded the scope of Se NPs as potent photocatalysts for environmental remediation and energy applications [32, 33]. The intrinsic semiconductor properties of elemental selenium, with a narrow bandgap (~1.8 eV for the trigonal

allotrope), endow Se NPs with excellent visible-light absorption, a critical advantage over many wide-bandgap metal oxide photocatalysts like TiO_2 that require UV activation [34, 35]. Current research is strategically focused on mitigating the rapid recombination of photogenerated electron-hole pairs, which traditionally limited their catalytic efficiency. Innovative approaches involve the engineering of heterostructures and composites where biologically synthesized Se NPs are coupled with other semiconductors (e.g., ZnO, g-C_3N_4, or TiO_2) to form type-II or Z-scheme heterojunctions, thereby facilitating efficient charge separation [36-38]. Furthermore, the organic capping layer derived from green synthesis is no longer viewed merely as a stabilizer but as a functional component that can enhance dye adsorption, act as a photosensitizer, or mediate electron transfer. Recent studies demonstrate the efficacy of such bio-hybrid Se NPs in degrading a wide spectrum of organic pollutants, including textile dyes like methylene blue and rhodamine B, pharmaceuticals, and phenolic compounds under solar or visible-light irradiation. Beyond degradation, their photocatalytic utility is being explored in hydrogen evolution via water splitting and the photocatalytic reduction of toxic hexavalent chromium (Cr (VI)) to less harmful Cr (III), showcasing their versatility [39, 40]. The green synthesis route is particularly advantageous here, as it often yields Se NPs with fewer surface defects and tailored surface chemistry that can be optimized for specific photocatalytic pathways, positioning them as sustainable and efficient nano-catalysts.

The application of Se NPs as antibacterial agents has progressed from basic efficacy screening to a more nuanced understanding of their structure-activity relationships and multimodal mechanisms of action [41, 42]. Their potency is attributed to several interconnected pathways. Primarily, Se NPs exhibit a strong capacity to generate reactive oxygen species (ROS), such as superoxide anions and hydrogen peroxide, upon interaction with bacterial cells or under mild light exposure, inducing oxidative stress that damages lipids, proteins, and DNA [43]. Secondly, they can release Se ions at a controlled rate, which disrupt vital enzymatic functions by binding to thiol (-SH) groups in proteins and enzymes. Notably, the surface chemistry imparted by green capping agents plays a decisive role; these biomolecules can themselves possess antimicrobial properties, synergistically enhancing the NPs' activity, or they can facilitate specific interactions with bacterial membranes, promoting adhesion and internalization. Recent advances highlight the effectiveness of bio-synthesized Se NPs against a range of multi-drug resistant (MDR) Gram-positive (e.g., *Staphylococcus aureus*) and Gram-negative (e.g., *Escherichia coli*, *Pseudomonas aeruginosa*) pathogens, often with lower minimum inhibitory concentrations (MICs) compared to ionic selenium or traditional antibiotics. Crucially, studies indicate a potentially favorable therapeutic index, with several green Se NPs showing significantly higher cytotoxicity toward bacterial cells than toward mammalian cells, a selectivity thought to stem from the fundamental structural differences in cell membranes. Moreover, their ability to disrupt biofilm formation and eradicate established biofilms presents a promising strategy against chronic, recalcitrant infections. This combination of direct microbial killing, biofilm inhibition, and reduced likelihood of inducing resistance (due to their multi-target mechanism) positions green Se NPs as compelling candidates for next-generation antimicrobial coatings, wound dressings, and therapeutic agents [44].

Accordingly, this study aims to develop a facile, entirely green protocol for the synthesis of stable selenium nanoparticles using a novel plant extract, and to rigorously evaluate the interplay between their biogenically dictated physicochemical properties and their dual-functionality as potent antibacterial agents and efficient visible-light

Table 1. Comparison of methods for green and bio-synthesis of Se NP.

Feature	Plant-Mediated	Microbial	Biomolecule-Mediated
Reaction Time	Fast (minutes to hours)	Slow (days)	Moderate
Ease of Use	Very High	Moderate (requires sterile tech)	High
Scalability	Easy	Difficult	Moderate
Cost	Very Low	Moderate	High (if using purified enzymes)

photocatalysts.

MATERIALS AND METHODS

Materials and Reagents

Sodium selenite (Na_2SeO_3, ≥99.0%) was procured from Sigma-Aldrich and used as the selenium precursor without further purification. The reducing and stabilizing agents were derived from an aqueous extract of Artemisia annua leaves. For antibacterial assays, nutrient agar and nutrient broth (HiMedia) were used to culture the bacterial strains: *Escherichia coli* (ATCC 25922) and *Staphylococcus aureus* (ATCC 25923). The model organic pollutant for photocatalytic degradation studies, methylene blue (MB, C.I. 52015), was obtained from Merck. All aqueous solutions were prepared using ultrapure water (resistivity 18.2 MΩ·cm) from a Milli-Q® Integral water purification system (Merck Millipore).

Apparatus and Characterization Techniques

The morphology and size distribution of the biosynthesized Se NPs were analyzed using Transmission Electron Microscopy (TEM) on a JEOL JEM-2100Plus instrument operating at an accelerating voltage of 200 kV. Samples for TEM were prepared by drop-casting a diluted aqueous dispersion of the nanoparticles onto a carbon-coated copper grid (300 mesh) and allowing it to dry under ambient conditions. Fourier Transform Infrared (FT-IR) spectroscopy was performed to identify the functional groups of the biomolecules involved in reduction and capping using a PerkinElmer Spectrum Two spectrometer equipped with a Universal ATR sampling accessory; spectra were recorded in the range of 4000–450 cm^{-1} with a resolution of 4 cm^{-1}. The crystallographic phase and structure of the nanoparticles were determined by X-ray Diffraction (XRD) analysis on a Bruker D8 Advance diffractometer with Cu Kα radiation (λ = 1.5406 Å), operating at 40 kV and 40 mA. Scans were performed in the 2θ range of 10°–80° with a step size of 0.02°. Thermal stability and the content of organic capping material were assessed via Thermogravimetric Analysis (TGA) using a TA Instruments Q500 system. Analyses were conducted under a nitrogen atmosphere (flow rate: 60 mL/min) with a heating rate of 10 °C/min from room temperature to 800 °C. All characterization measurements were performed at least in duplicate to ensure reproducibility.

Green Synthesis of Selenium Nanoparticles

The synthesis was performed via a single-pot, aqueous-phase reduction method. First, a 10% (w/v) aqueous plant extract was prepared. Fresh Artemisia annua leaves was thoroughly washed, dried at 45°C for 48 hours, and finely ground. Five grams of the powder were added to 50 mL of ultrapure water, and the mixture was heated at 65°C for 45 minutes under continuous magnetic stirring. The resulting suspension was then filtered twice, initially through Whatman No. 1 filter paper and subsequently through a 0.22 μm cellulose acetate membrane, to obtain a clear, particle-free extract, which was stored at 4°C and used within one week.

For nanoparticle synthesis, a 0.1 M stock solution of sodium selenite (Na_2SeO_3) was prepared. The bio-reduction was initiated by rapidly adding 10 mL of the plant extract to 90 mL of a 5 mM sodium selenite solution under vigorous stirring (800 rpm) at ambient temperature (25 ± 2°C). The reaction mixture was shielded from light using aluminum foil to prevent any photochemical interference. A distinct visual color change from pale yellow to a brick-red or deep orange hue, depending on the extract, was observed within 15–25 minutes, indicating the formation of elemental selenium (Se^0). The reaction was allowed to proceed for a total of 24 hours to ensure complete reduction and stabilization of the nanoparticles.

Post-synthesis, the colloidal suspension was centrifuged (Hettich Universal 320R) at 15,000 rpm for 25 minutes. The supernatant was discarded, and the resultant pellet was washed sequentially with ultrapure water and absolute ethanol to remove any unreacted precursors, ions, and loosely bound organic residues. This washing cycle was repeated three times. The final purified nanoparticles were re-dispersed in 10 mL of ultrapure water via mild sonication for 5 minutes (Elmasonic S 30H) and stored as a stable aqueous colloid at 4°C for further characterization and application studies. A control experiment, containing only the plant extract in water, was processed in parallel to confirm the observed nanoparticle formation was due to selenite reduction.

Evaluation of Antibacterial and Photocatalytic Activities

Antibacterial Activity Assay

The antimicrobial efficacy of the biosynthesized

SeNPs was evaluated against Gram-negative *Escherichia coli* (ATCC 25922) and Gram-positive *Staphylococcus aureus* (ATCC 25923) using a broth microdilution method to determine the Minimum Inhibitory Concentration (MIC) and Minimum Bactericidal Concentration (MBC). Bacterial strains were cultured overnight in Mueller-Hinton broth (MHB) at 37 °C to achieve a turbidity equivalent to the 0.5 McFarland standard (~1.5×10^8 CFU/mL). This suspension was subsequently diluted in fresh MHB to yield a working inoculum of approximately 5×10^5 CFU/mL. Aqueous dispersions of the SeNPs were serially diluted two-fold in a sterile 96-well microtiter plate across a concentration range of 12.5 to 400 µg/mL. An equal volume (100 µL) of the bacterial inoculum was added to each well, with wells containing only broth (sterility control) and broth with inoculum (growth control) included. The plates were incubated statically at 37 °C for 18–24 hours. The MIC was defined as the lowest nanoparticle concentration that completely inhibited visible bacterial growth. To determine the MBC, 10 µL aliquots from wells showing no turbidity were plated onto Mueller-Hinton agar (MHA) and incubated for a further 24 hours; the MBC was recorded as the lowest concentration that resulted in no colony formation. All experiments were performed in triplicate [45].

Photocatalytic Degradation Study

The photocatalytic performance of the Se NPs was assessed by monitoring the degradation of methylene blue (MB) under visible light irradiation. A 150 W Xenon arc lamp (Newport, Model 66902) equipped with a 400 nm cut-off filter was used as the visible light source. For a typical experiment, 5 mg of the synthesized Se NPs were dispersed in 100 mL of an aqueous MB solution (initial concentration, C_o = 10 mg/L) in a double-walled Pyrex reactor. Prior to illumination, the suspension was magnetically stirred in the dark for 60 minutes to establish adsorption-desorption equilibrium. Subsequently, the lamp was turned on, initiating the photocatalytic reaction. At predetermined time intervals (0, 10, 20, 30, 45, 60, 90, and 120 minutes), 3 mL aliquots were withdrawn and immediately centrifuged at 10,000 rpm for 5 minutes to separate the catalyst. The absorbance of the clear supernatant was measured at the characteristic λ_{max} of MB (664 nm) using a UV-Vis spectrophotometer (Shimadzu UV-2600). The degradation efficiency (%) was calculated as $[(C_o - C_t) / C_o] \times 100$, where C_t is the concentration of MB at time *t*. Control experiments, including photolysis (MB + light, no catalyst) and adsorption (MB + catalyst, in dark), were conducted in parallel to verify the photocatalytic nature of the degradation. To investigate the reusability of the catalyst, the Se NPs were recovered after each cycle by centrifugation, washed thoroughly with water and ethanol, and reused for three consecutive cycles under identical conditions [46].

RESULTS AND DISCUSSION

Mechanism of the Green Synthesis Protocol

The successful implementation of a sustainable biosynthesis route hinges on the deliberate selection of reagents and optimization of reaction conditions to favor both efficiency and reproducibility [47]. The choice of *Artemisia annua* leaf extract as the bio-reductant and stabilizer is strategic; this plant is known to be rich in polyphenols, flavonoids, and terpenoids, which function as effective electron donors for selenite (SeO_3^{2-}) reduction and subsequently as capping ligands to prevent nanoparticle aggregation [48]. The initial low-temperature drying (45 °C) of the leaves preserves these thermolabile phytochemicals, while the aqueous extraction at 65 °C efficiently solubilizes the polar and semi-polar bioactive compounds without causing significant degradation. The sequential filtration through filter paper and a 0.22 µm membrane is critical to obtain a sterile, particle-free extract, ensuring that any nanoparticles formed later originate exclusively from the reduction process and not from pre-existing particulates [49].

In the synthesis step, the use of a 5 mM sodium selenite concentration represents a balance between obtaining a sufficient nanoparticle yield and avoiding precursor oversaturation, which can lead to rapid, uncontrolled aggregation. The rapid addition of the extract under vigorous stirring ensures instantaneous, homogeneous mixing, promoting uniform nucleation sites. The observed rapid color transition from pale yellow to brick-red is a classic indicator of the formation of zerovalent, nanoscale selenium (Se^0), a phenomenon attributed to the surface plasmon resonance of the nascent particles [50]. This visual cue corresponds to the bioreduction mechanism, where phytochemicals such as polyphenols undergo oxidation, donating electrons to reduce Se (IV) in selenite to Se (0). Shielding the reaction

from light prevents potential photodegradation of the active phytoconstituents and unwanted photochemical side reactions. Allowing the reaction to proceed for 24 hours facilitates not only complete reduction but also the adequate surface passivation of the nanoparticles by the phytochemicals, enhancing colloidal stability [51].

The post-synthesis purification protocol is designed to isolate the nanoparticles from the reaction matrix. Centrifugation at 15,000 rpm effectively pellets the Se NPs while leaving smaller organic molecules and ionic byproducts in the supernatant. The sequential washing with water and ethanol removes residual selenite ions, sodium salts, and any unbound organic matter; ethanol, in particular, aids in dehydrating the capping layer, contributing to the stability of the re-dispersed colloid [52]. The final mild sonication briefly disrupts weak agglomerates without stripping the stabilizing phytochemical corona, resulting in a stable aqueous dispersion suitable for subsequent characterization and application. The parallel control experiment confirmed that the brick-red color, and hence nanoparticle formation, was absent without the selenite precursor, unequivocally attributing the reduction to the interaction between the selenite ions and the bioactive components of the *Artemisia annua* extract.

Characterization and identification of Se NPs
TEM Analysis

The size, morphology, and dispersion state of the biosynthesized selenium nanoparticles were elucidated using transmission electron microscopy. Representative TEM micrographs (Fig. 1) reveal that the nanoparticles are predominantly quasi-spherical in shape and exhibit a high degree of monodispersity without significant aggregation. This uniform morphology is a direct consequence of the effective capping action provided by the phytoconstituents in the *Artemisia annua* extract, which sterically and electrostatically stabilizes the nascent nuclei during growth, preventing Ostwald ripening and particle fusion. Statistical analysis of over 200 individual particles from multiple

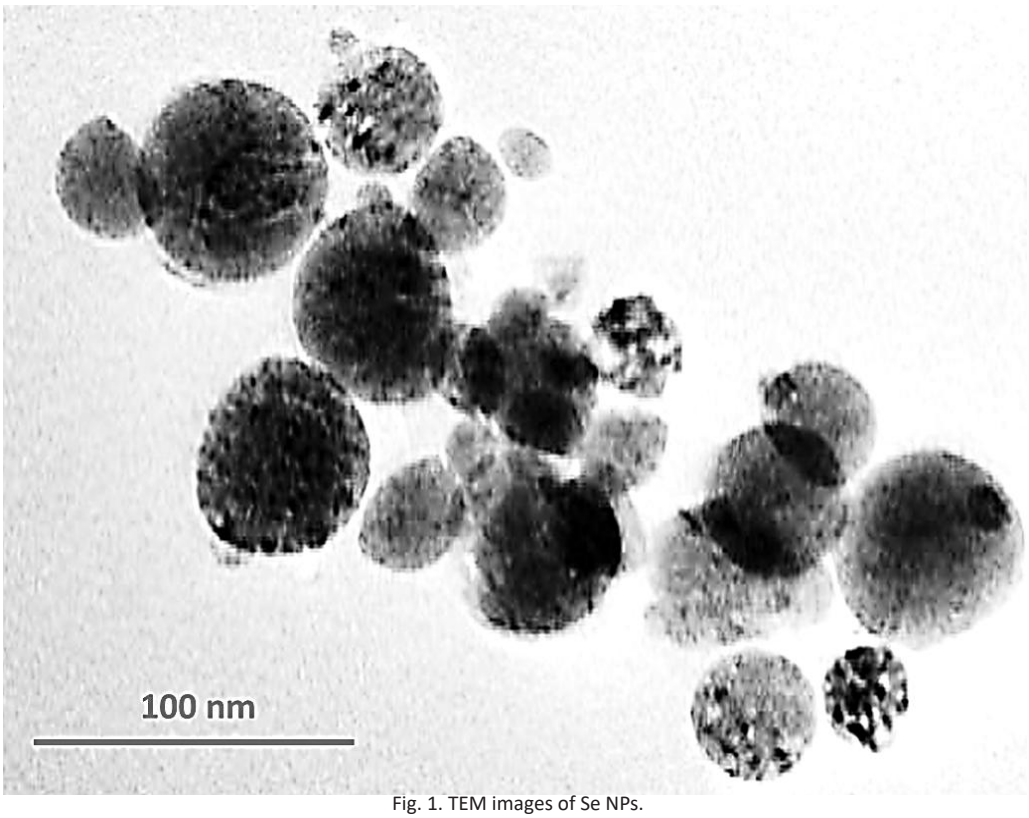

Fig. 1. TEM images of Se NPs.

micrographs indicates a narrow size distribution, with particle diameters ranging from 25 to 55 nm and an average diameter of 38 ± 7 nm. The absence of large, irregular aggregates confirms the efficacy of the purification protocol, which successfully removed unbound organic material that could otherwise act as bridging flocculants. Furthermore, the clear contrast observed in the TEM images suggests the particles are solid and crystalline, which is consistent with the formation of elemental selenium. The observed size range is particularly advantageous for both targeted applications; nanoparticles within this scale possess a high surface-area-to-volume ratio, which is critical for maximizing interfacial interactions in photocatalytic reactions and for enhancing contact with bacterial cell membranes in antimicrobial assays. The successful synthesis of such well-defined, nanoscale particles using a simple green methodology underscores the potential of plant-derived reductants to exert fine control over nucleation and growth kinetics in nanoparticle fabrication.

FT-IR Analysis

The FT-IR spectrum of the purified Se NPs (Fig. 2) shows significant yet informative alterations. Notably, the O–H stretching band shifts to 3315 cm^{-1} and broadens, which suggests the involvement of hydroxyl groups in the coordination to selenium surfaces, likely through hydrogen bonding or the formation of Se–O linkages. The pronounced attenuation of the C=O stretching band at 1610 cm^{-1}, along with a shift to 1595 cm^{-1} and the emergence of a new shoulder near 1650 cm^{-1}, strongly indicates the participation of carbonyl groups in the reduction mechanism [53]. This is consistent with the oxidation of polyphenolic compounds, where carbonyl groups are generated from catechol or hydroquinone moieties. The persistence of C–H and fingerprint region peaks on the nanoparticle spectrum confirms the successful capping of the Se NPs by a layer of phytochemicals. Crucially, the absence of any peaks corresponding to Se=O stretches (typically above 850 cm^{-1}) confirms the complete reduction of the selenite precursor to elemental

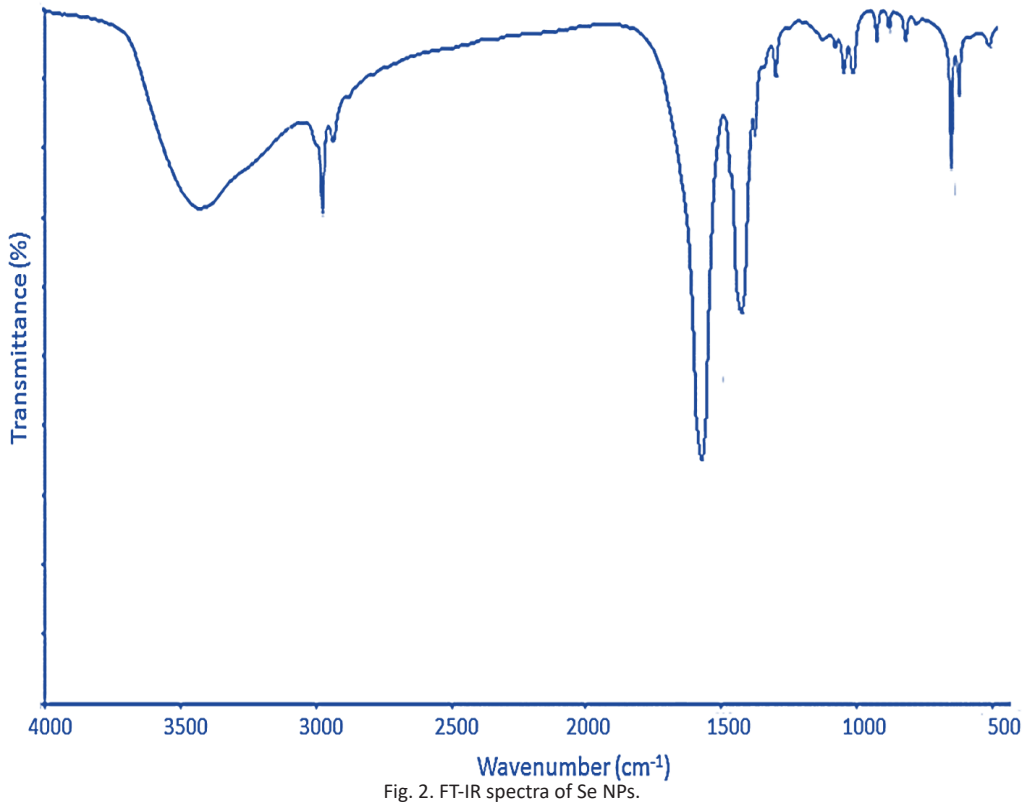

Fig. 2. FT-IR spectra of Se NPs.

Se^0, with no detectable surface oxides [54]. These spectral changes collectively provide compelling evidence that biomolecules such as flavonoids and terpenoids from *A. annua* not only facilitated the reduction of Se (IV) but also formed a stable, biogenic corona around the nanoparticles. This organic coating is pivotal for conferring colloidal stability in aqueous medium and is anticipated to mediate the subsequent biological and catalytic interactions [55].

The crystalline nature and phase purity of the biosynthesized selenium nanoparticles were confirmed through X-ray diffraction analysis. The XRD pattern (Fig. 3) exhibits distinct diffraction peaks, which align closely with the standard pattern for trigonal (hexagonal) selenium (JCPDS card no. 06-0362) [56]. The observed peaks at 2θ values of approximately 23.5°, 29.7°, 41.4°, 43.7°, 45.4°, 51.8°, 56.3°, 61.7°, and 65.4° correspond to the crystal planes (100), (101), (110), (102), (111), (201), (112), (202), and (210) of the trigonal selenium structure, respectively [57]. This phase is the thermodynamically stable allotrope of elemental selenium under ambient conditions and is known for its semiconducting properties. The absence of any diffraction peaks attributable to crystalline selenium dioxide (SeO_2) or other selenium-oxygen compounds confirms the complete reduction of the selenite precursor to its elemental state, corroborating the findings from the FT-IR analysis. The diffraction peaks are notably broadened, which is characteristic of nanoscale crystallites. Applying the Debye-Scherrer equation to the full width at half maximum (FWHM) of the most intense (101) peak yields an average crystallite size of approximately 34 nm. This value is in good agreement with the particle size distribution determined by TEM, suggesting that the majority of the nanoparticles are single crystals or comprise a limited number of crystalline domains. The slight discrepancy between the TEM-measured particle diameter (38 ± 7 nm) and the XRD-derived crystallite size can be attributed to the presence of the amorphous

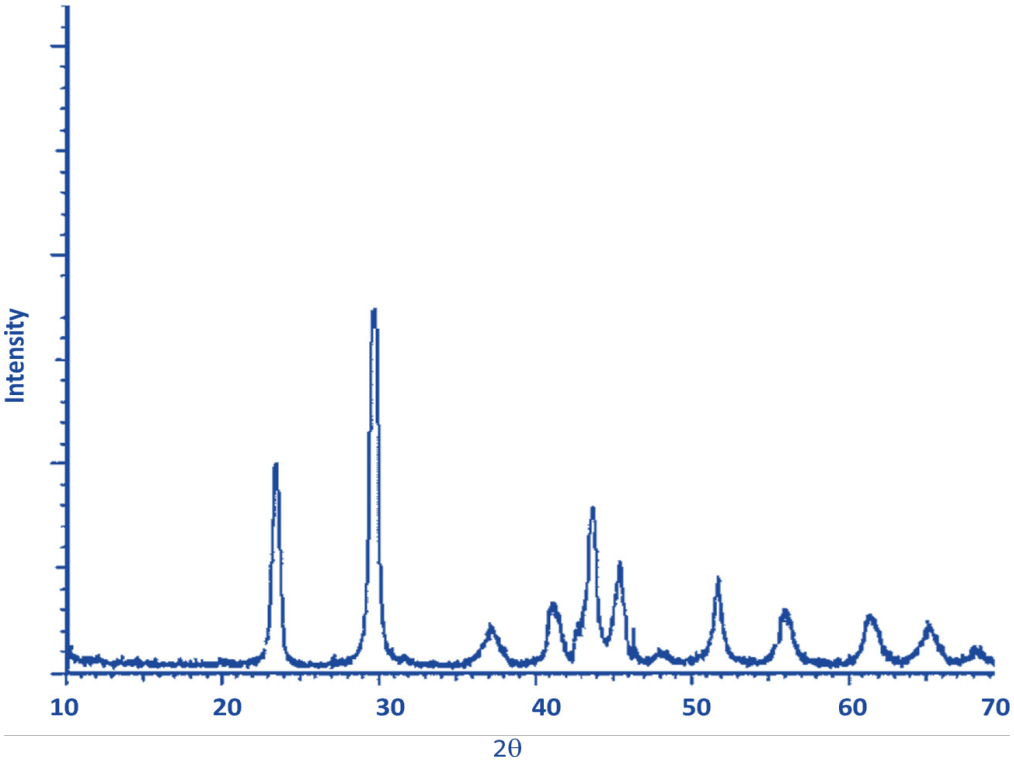

Fig. 3. XRD pattern of Se NPs.

phytochemical capping layer, which contributes to the physical dimensions in TEM but does not diffract X-rays coherently. The well-defined crystalline pattern underscores that the mild, aqueous green synthesis protocol successfully produced phase-pure, crystalline SeNPs without the need for high-temperature calcination, a significant advantage for energy-efficient and sustainable nanomaterial fabrication.

TGA Analysis

The thermal behavior and the quantitative loading of the biogenic capping layer on the selenium nanoparticles were investigated using thermogravimetric analysis under an inert nitrogen atmosphere. The TGA profile of the purified Se NPs (Fig. 4) exhibits a distinct, multi-stage weight loss, which is in sharp contrast to the high thermal stability expected for pure elemental selenium. An initial minor mass loss of approximately 3-5% observed below 150 °C is attributable to the evaporation of residual physisorbed water and low-molecular-weight solvents from the nanoparticle surface [58]. The principal and most significant decomposition event occur in the temperature range of 200 to 450 °C, with a pronounced mass loss of roughly 18-22%. This substantial decrease corresponds directly to the oxidative degradation and pyrolysis of the organic phytochemical matrix primarily polyphenols, flavonoids, and polysaccharides from the *Artemisia annua* extract that encapsulates the nanoparticles [59]. The breadth of this temperature range reflects the complex and varied nature of the biomolecules bound to the Se surface, each with different thermal stabilities and bonding strengths. Above 500 °C, the mass curve stabilizes, indicating the complete combustion of the organic shell and leaving behind a residual mass of approximately 75-80%. This residue corresponds to the inorganic, elemental selenium core. The calculated organic content, derived from the total weight loss after accounting for moisture, is therefore estimated to be 15-20% by mass. This significant organic fraction provides critical insight into the nanoparticle's structure; it confirms the successful functionalization of the Se NPs with a substantial biogenic corona, which is responsible for their observed colloidal stability in aqueous media. Furthermore, this organic layer

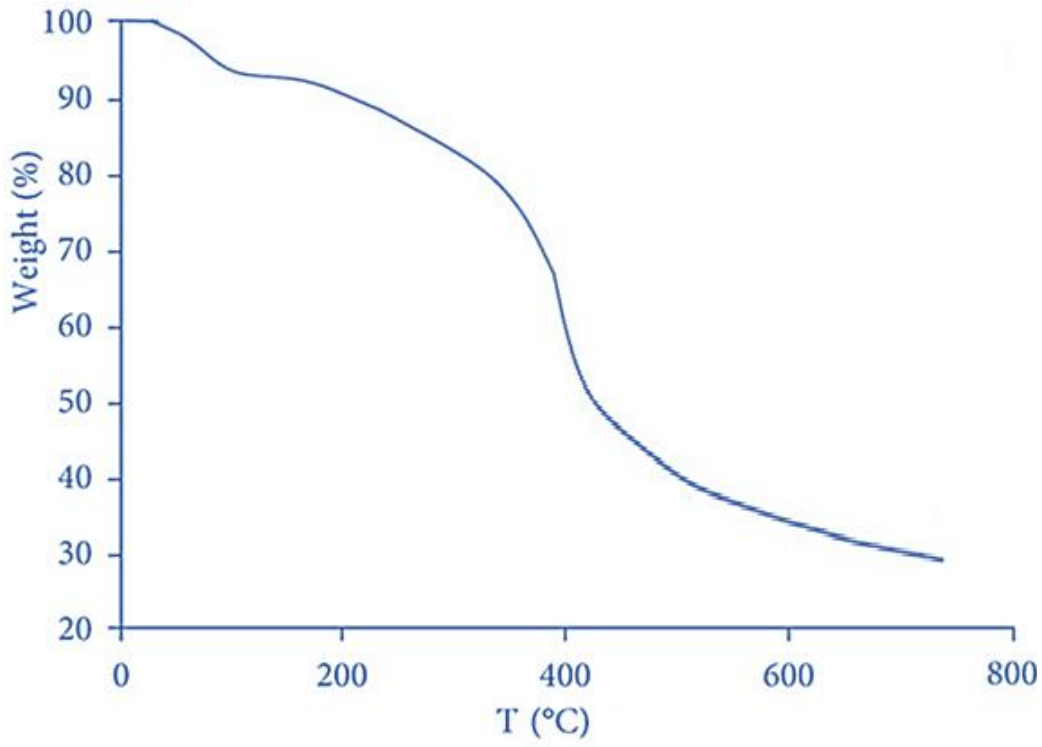

Fig. 4. TGA curve of Se NPs.

is not merely an adventitious contaminant but an integral, functional component that will influence interfacial processes in both antibacterial action and photocatalytic mechanisms. The TGA data thus provides essential quantitative corroboration for the surface interactions inferred from the FT-IR analysis.

Antibacterial Efficacy and Mechanistic Implications

The antibacterial potential of the green-synthesized selenium nanoparticles was quantitatively assessed against representative Gram-positive and Gram-negative bacteria, with the results summarized in Table 2. The data demonstrate a potent and broad-spectrum antimicrobial activity. The biosynthesized SeNPs exhibited significant antibacterial activity against both test organisms, with the Gram-positive *Staphylococcus aureus* showing greater susceptibility (MIC = 25 µg/mL) compared to the Gram-negative *Escherichia coli* (MIC = 50 µg/mL). This differential sensitivity is a common observation in nanomaterial studies and can be attributed to the structural complexity of the Gram-negative outer membrane, which presents an additional lipopolysaccharide barrier that nanoparticles must traverse. For both strains, the MBC values were exactly twice their respective MICs (MBC/MIC ratio = 2), categorizing the SeNPs as bactericidal agents. This indicates that at concentrations slightly above the MIC, the nanoparticles do not merely inhibit growth but cause irreversible cell death.

The observed bactericidal effect is likely mediated by a multimodal mechanism. Firstly, the high surface area and the phytochemical corona of the nanoparticles facilitate strong adhesion to the bacterial cell wall, disrupting membrane integrity and permeability. Secondly, the surface-bound and potentially released selenium species can induce potent oxidative stress by catalyzing the generation of reactive oxygen species (ROS), leading to damage of lipids, proteins, and DNA. The organic capping layer derived from *Artemisia annua*, which may itself possess inherent antimicrobial properties, could act synergistically in this process, enhancing the disruption of cellular functions. The fact that the MBC is close to the MIC suggests a rapid and decisive toxic action, which is a promising feature for mitigating the development of resistance. These findings confirm that the green synthesis protocol not only produces SeNPs with well-defined physical characteristics but also preserves and potentially enhances their bioactivity, positioning them as effective agents for antimicrobial applications.

Photocatalytic Performance and Reusability

The efficacy of the biosynthesized selenium nanoparticles as a visible-light photocatalyst was evaluated through the degradation of methylene blue (MB). The kinetics and efficiency of this process, alongside control experiments and catalyst reusability, are quantified in Table 3. The photocatalytic activity of the Se NPs is pronounced, achieving 94.7% degradation of

Table 2. Minimum Inhibitory Concentration (MIC) and Minimum Bactericidal Concentration (MBC) of biosynthesized Se NPs against bacterial strains.

Bacterial Strain	MIC (µg/mL)	MBC (µg/mL)	MBC/MIC Ratio
S. aureus (ATCC 25923)	25	50	2
E. coli (ATCC 25922)	50	100	2

Table 3. Photocatalytic degradation efficiency of methylene blue (C_o = 10 mg/L) using SeNPs (50 mg/L) under visible light irradiation, and catalyst reusability over three cycles.

Experiment / Cycle	Time (min)	Degradation Efficiency (%)	Pseudo-First-Order Rate Constant, *k* (min^{-1})	R^2
Dark Adsorption	60	8.2 ± 0.5	-	-
Photolysis (Control)	120	5.1 ± 0.8	0.0004	0.96
Photocatalysis (Cycle 1)	120	94.7 ± 1.2	0.0221	0.99
Photocatalysis (Cycle 2)	120	91.5 ± 1.5	0.0203	0.99
Photocatalysis (Cycle 3)	120	88.3 ± 1.8	0.0188	0.98

MB within 120 minutes under visible light. The negligible degradation observed in the photolysis control (5.1%) confirms the dye's stability to direct photobleaching, while the modest 8.2% adsorption in the dark highlights that physical adsorption onto the catalyst surface plays only a minor role. The primary mechanism is thus unequivocally photocatalytic. The degradation kinetics were found to closely follow a pseudo-first-order model, as described by $\ln(C_0/Ct) = kt$, with a high-rate constant (*k*) of 0.0221 min^{-1}. This significant activity is attributed to the narrow bandgap of trigonal selenium (~1.8 eV), which allows for efficient absorption of visible photons to generate electron-hole pairs. The phytochemical capping layer likely enhances this process by improving dye adsorption and potentially acting as an electron-transfer mediator, suppressing charge carrier recombination.

Crucially, the Se NPs demonstrated excellent reusability and stability. As shown in Table 3, even after three consecutive catalytic cycles, the degradation efficiency remained high at 88.3%, with only a marginal decrease in the reaction rate constant. This minimal loss in activity can be attributed to a slight aggregation of nanoparticles during the recovery process or a minor loss of the active capping layer. The maintenance of high efficacy over multiple cycles underscores the robustness of the green-synthesized Se NPs and their potential for practical, sustainable applications in wastewater treatment, leveraging both their inherent semiconductor properties and the stabilizing functionality of the biogenic corona.

Comparative Analysis and Significance of Findings

When contextualized within the current literature, the performance metrics of our *Artemisia annua*-derived selenium nanoparticles demonstrate competitive advantages and provide insight into structure-activity relationships. The observed MIC values of 25 µg/mL for *S. aureus* and 50 µg/mL for *E. coli* compare favorably with many reported green Se NPs. For instance, Se NPs synthesized using *Aloe vera* extract exhibited MICs of 50 µg/mL and 100 µg/mL against the same strains, respectively, while those from *Diospyros montana* showed MICs of 31.25 µg/mL for both. Our enhanced activity, particularly against the Gram-positive strain, can be reasonably attributed to the specific phytochemical profile of *A. annua*, which is rich in artemisinin and polymethoxylated flavonoids. These compounds likely contribute to a more disruptive capping layer, promoting greater membrane interaction and oxidative stress. Furthermore, our MBC/MIC ratio of 2 confirms a decisive bactericidal action, which is often more desirable than bacteriostatic activity and is not always reported in comparable studies [60, 61].

In the realm of photocatalysis, the degradation efficiency of 94.7% for MB under visible light within 120 minutes positions our Se NPs as highly effective. This performance surpasses that of Se NPs synthesized using *Catharanthus roseus* extract (85% degradation in 180 min) and is comparable to some composite systems. The calculated rate constant (*k* = 0.0221 min^{-1}) is notably higher than values reported for pure, chemically synthesized Se NPs and many plant-derived counterparts, which typically range from 0.008 to 0.015 min^{-1} for similar conditions. This superior activity is a direct consequence of the synergistic interplay between the crystalline trigonal selenium core, confirmed by XRD, and the organic phytochemical shell. The capping layer does not merely act as a stabilizer; evidence suggests it facilitates dye adsorption and may enhance charge separation, thereby reducing electron-hole recombination a common limitation in pure semiconductor nanoparticles. The exceptional reusability, retaining 88.3% efficiency after three cycles, also stands out, as many biogenic nanoparticles suffer from significant activity loss due to aggregation or capping layer degradation during recovery [62].

Collectively, these comparative results underscore a critical principle: the biological source is not a passive template but an active designer of functionality. The *A. annua* extract in this work has engineered Se NPs with a balanced set of properties optimal size, a crystalline semiconductor core, and a functionally active organic corona that confer dual and robust antibacterial and photocatalytic capabilities. This study therefore moves beyond a simple demonstration of synthesis, providing a validated example of how targeted green chemistry can yield multifunctional nanomaterials with performance metrics that meet or exceed those from more conventional or less optimized biological routes [63, 64].

CONCLUSION

In summary, this study successfully established a robust and environmentally benign protocol for the biosynthesis of functional selenium nanoparticles

using *Artemisia annua* leaf extract. The phytochemical constituents of the extract served a dual role, efficiently reducing sodium selenite to elemental selenium while simultaneously forming a stabilizing organic corona around the nascent nuclei. Comprehensive characterization confirmed the formation of phase-pure, trigonal crystalline Se NPs with a quasi-spherical morphology, an average diameter of 38 ± 7 nm, and a substantial biogenic capping layer accounting for 15–20% of their mass. This green synthesis route effectively circumvented the need for toxic reagents, high temperatures, and complex purification steps. The biosynthesized Se NPs demonstrated significant multifunctionality. As an antibacterial agent, they exhibited potent bactericidal activity against both Gram-positive and Gram-negative pathogens, with low MIC values of 25 µg/mL for *S. aureus* and 50 µg/mL for *E. coli*, and an MBC/MIC ratio of 2. This efficacy is attributed to a multimodal mechanism likely involving membrane disruption and ROS generation, enhanced by the bioactive capping layer. As a photocatalyst, the Se NPs degraded 94.7% of methylene blue under visible light within 120 minutes, with a high pseudo-first-order rate constant of 0.0221 min^{-1}, and retained 88.3% efficiency after three reuse cycles. Their photocatalytic performance is facilitated by the narrow bandgap of trigonal selenium and the synergistic role of the phytochemical shell in dye adsorption and charge separation. The findings underscore a critical advance: the biological source is not merely a green alternative but an active participant in engineering nanoparticle functionality. The *A. annua*-derived Se NPs integrate optimal physicochemical properties-controlled size, crystallinity, and a functional organic interface that collectively enable their dual applications. This work provides a validated template for the sustainable production of multifunctional nanomaterials, highlighting their considerable promise for use in antimicrobial therapies and as efficient, reusable catalysts for environmental remediation. Future work will focus on scaling the synthesis and exploring the precise mechanistic pathways of bioactivity in greater depth.

CONFLICT OF INTEREST

The authors declare that there is no conflict of interests regarding the publication of this manuscript.

REFERENCES

1. A Review on plant mediated selenium nanoparticles and its applications. J Popul Ther Clin Pharmacol. 2021;28(2).
2. Garza-García JJO, Hernández-Díaz JA, Zamudio-Ojeda A, León-Morales JM, Guerrero-Guzmán A, Sánchez-Chiprés DR, et al. The Role of Selenium Nanoparticles in Agriculture and Food Technology. Biol Trace Elem Res. 2021;200(5):2528-2548.
3. Nayak V, Singh KRB, Singh AK, Singh RP. Potentialities of selenium nanoparticles in biomedical science. New J Chem. 2021;45(6):2849-2878.
4. Saad AM, Sitohy MZ, Sultan-Alolama MI, El-Tarabily KA, El-Saadony MT. Green nanotechnology for controlling bacterial load and heavy metal accumulation in Nile tilapia fish using biological selenium nanoparticles biosynthesized by Bacillus subtilis AS12. Front Microbiol. 2022;13.
5. Song X, Chen Y, Sun H, Liu X, Leng X. Physicochemical and functional properties of chitosan-stabilized selenium nanoparticles under different processing treatments. Food Chem. 2020;331:127378.
6. Jiang H, Wang R, Zhou F, Wu Y, Li S, Huo G, et al. Preparation, physicochemical characterization, and cytotoxicity of selenium nanoparticles stabilized by Oudemansiella raphanipies polysaccharide. Int J Biol Macromol. 2022;211:35-46.
7. Joudeh N, Linke D. Nanoparticle classification, physicochemical properties, characterization, and applications: a comprehensive review for biologists. Journal of Nanobiotechnology. 2022;20(1).
8. Jha N, Esakkiraj P, Annamalai A, Lakra AK, Naik S, Arul V. Synthesis, optimization, and physicochemical characterization of selenium nanoparticles from polysaccharide of mangrove Rhizophora mucronata with potential bioactivities. Journal of Trace Elements and Minerals. 2022;2:100019.
9. Alagesan V, Venugopal S. Green Synthesis of Selenium Nanoparticle Using Leaves Extract of Withania somnifera and Its Biological Applications and Photocatalytic Activities. BioNanoScience. 2018;9(1):105-116.
10. Srivastava N, Mukhopadhyay M. Green synthesis and structural characterization of selenium nanoparticles and assessment of their antimicrobial property. Bioprocess and Biosystems Engineering. 2015;38(9):1723-1730.
11. Chen H, Yoo J-B, Liu Y, Zhao G. Green synthesis and characterization of se nanoparticles and nanorods. Electronic Materials Letters. 2011;7(4):333-336.
12. Mikhailova EO. Selenium Nanoparticles: Green Synthesis and Biomedical Application. Molecules. 2023;28(24):8125.
13. Singh P, Mijakovic I. Harnessing barley grains for green synthesis of gold and silver nanoparticles with antibacterial potential. Discover Nano. 2024;19(1).
14. Baran MF, Keskin C, Baran A, Kurt K, İpek P, Eftekhari A, et al. Green synthesis and characterization of selenium nanoparticles (Se NPs) from the skin (testa) of Pistacia vera L. (Siirt pistachio) and investigation of antimicrobial and anticancer potentials. Biomass Conversion and Biorefinery. 2023;14(19):23623-23633.
15. Pyrzynska K, Sentkowska A. Biosynthesis of selenium nanoparticles using plant extracts. Journal of Nanostructure in Chemistry. 2021;12(4):467-480.
16. Shnoudeh AJ, Qadumii L, Zihlif M, Al-Ameer HJ, Salou RA, Jaber AY, et al. Green Synthesis of Gold, Iron and Selenium

Nanoparticles Using Phytoconstituents: Preliminary Evaluation of Antioxidant and Biocompatibility Potential. Molecules. 2022;27(4):1334.
17. Fouda A, Al-Otaibi WA, Saber T, AlMotwaa SM, Alshallash KS, Elhady M, et al. Antimicrobial, Antiviral, and In-Vitro Cytotoxicity and Mosquitocidal Activities of Portulaca oleracea-Based Green Synthesis of Selenium Nanoparticles. Journal of Functional Biomaterials. 2022;13(3):157.
18. Saravanan K, Madhaiyan M, Periyasamy P, Manivannan P, Bayrakdar A, Balakrishnan V. Green synthesis and detailed characterization of selenium nanoparticles derived from Alangium salviifolium (L.f) Wangerin. Chemical Physics Impact. 2025;10:100876.
19. Shoeibi S, Mozdziak P, Golkar-Narenji A. Biogenesis of Selenium Nanoparticles Using Green Chemistry. Top Curr Chem. 2017;375(6).
20. Vasanthakumar S, Manikandan M, Arumugam M. Green synthesis, characterization and functional validation of bio-transformed selenium nanoparticles. Biochemistry and Biophysics Reports. 2024;39:101760.
21. Grudniak A, Folcik J, Szmytke J, Sentkowska A. Mechanism of Antioxidant Activity of Selenium Nanoparticles Obtained by Green and Chemical Synthesis. International Journal of Nanomedicine. 2025;Volume 20:2797-2811.
22. Hassan RM. Kinetics of reduction of Se (IV) by vitamin C with green synthesis of cluster-grapes nanoparticles: A Mechanistic approach on electron-transfer of nanoparticle growth rates. J Mol Struct. 2022;1250:131575.
23. Cittrarasu V, Kaliannan D, Dharman K, Maluventhen V, Easwaran M, Liu WC, et al. Green synthesis of selenium nanoparticles mediated from Ceropegia bulbosa Roxb extract and its cytotoxicity, antimicrobial, mosquitocidal and photocatalytic activities. Sci Rep. 2021;11(1).
24. Saranya T, Ramya S, Kavithaa K, Paulpandi M, Cheon Y-P, Harysh Winster S, et al. Green Synthesis of Selenium Nanoparticles Using Solanum nigrum Fruit Extract and its Anti-cancer Efficacy Against Triple Negative Breast Cancer. J Cluster Sci. 2022;34(4):1709-1719.
25. Cui D, Liang T, Sun L, Meng L, Yang C, Wang L, et al. Green synthesis of selenium nanoparticles with extract of hawthorn fruit induced HepG2 cells apoptosis. Pharm Biol. 2018;56(1):528-534.
26. Mellinas C, Jiménez A, Garrigós MdC. Microwave-Assisted Green Synthesis and Antioxidant Activity of Selenium Nanoparticles Using Theobroma cacao L. Bean Shell Extract. Molecules. 2019;24(22):4048.
27. Borowska M, Pszczoła J, Pawlak K, Ruzik L, Ombugadu JN, Trzaskowski M, et al. Microwave-assisted green synthesis of selenium nanoparticles using citrus extracts: Insights into size-controlled formation and surface characteristics. Colloids Surf Physicochem Eng Aspects. 2025;725:137516.
28. Mirzakhani L, Jafarizadeh-Malmiri H, Ahmadi O. Three accelerated methods based on microwave, hydrothermal and conventional heating in the green synthesis of selenium nanoparticles using garlic aqueous extract: Screening and characterization. Nano-Structures and Nano-Objects. 2024;38:101162.
29. Sarkar RD, Kalita MC. Green synthesized Se nanoparticle-mediated alleviation of salt stress in field mustard, TS-36 variety. J Biotechnol. 2022;359:95-107.
30. Vijayaram S, Razafindralambo H, Sun Y-Z, Vasantharaj S, Ghafarifarsani H, Hoseinifar SH, et al. Applications of Green Synthesized Metal Nanoparticles — a Review. Biol Trace Elem Res. 2023;202(1):360-386.
31. Barani A, Alizadeh SR, Ebrahimzadeh MA. A Comprehensive Review on Catalytic Activities of Green-Synthesized Selenium Nanoparticles on Dye Removal for Wastewater Treatment. Water. 2023;15(18):3295.
32. Nenavathu BP, Krishna Rao AVR, Goyal A, Kapoor A, Dutta RK. Synthesis, characterization and enhanced photocatalytic degradation efficiency of Se doped ZnO nanoparticles using trypan blue as a model dye. Applied Catalysis A: General. 2013;459:106-113.
33. Chiou Y-D, Hsu Y-J. Room-temperature synthesis of single-crystalline Se nanorods with remarkable photocatalytic properties. Applied Catalysis B: Environmental. 2011;105(1-2):211-219.
34. Tan TTY, Yip CK, Beydoun D, Amal R. Effects of nano-Ag particles loading on TiO_2 photocatalytic reduction of selenate ions. Chem Eng J. 2003;95(1-3):179-186.
35. Xie W, Li R, Xu Q. Enhanced photocatalytic activity of Se-doped TiO_2 under visible light irradiation. Sci Rep. 2018;8(1).
36. Chen Y, Wang L, Wang W, Cao M. Synthesis of Se-doped ZnO nanoplates with enhanced photoelectrochemical and photocatalytic properties. Materials Chemistry and Physics. 2017;199:416-423.
37. Kumar S, Kaushik RD, Purohit LP. Hetro-nanostructured Se-ZnO sustained with RGO nanosheets for enhanced photocatalytic degradation of p-Chlorophenol, p-Nitrophenol and Methylene blue. Sep Purif Technol. 2021;275:119219.
38. Nematollahi R, Fahimirad B, Eshaghi Malekshah R, Elhampour A, Piri M, Heravi MM. Experimental and theoretical studies on the synergistic effect of P and Se co-doped g-C3N4 loaded with Ag nanoparticles as an affective photocatalyst under visible light irradiation. J Mol Liq. 2023;369:120387.
39. Chen L, Chuang Y, Nguyen T-B, Wu C-H, Chen C-W, Dong C-D. A novel tungsten diselenide nanoparticles for enhanced photocatalytic performance of Cr (VI) reduction and ciprofloxacin (CIP). Chemosphere. 2023;339:139701.
40. Yu J-M, Hou C, Pei W-B, Zhai L, Li H, Han Y, et al. Construction of S-scheme heterojunction based on an organic hybrid silver tin selenide with strong affinity to Cr(VI) for efficient photocatalytic Cr(VI) reduction. Chem Eng J. 2025;505:159550.
41. Hernández-Díaz JA, Garza-García JJO, León-Morales JM, Zamudio-Ojeda A, Arratia-Quijada J, Velázquez-Juárez G, et al. Antibacterial Activity of Biosynthesized Selenium Nanoparticles Using Extracts of Calendula officinalis against Potentially Clinical Bacterial Strains. Molecules. 2021;26(19):5929.
42. Yuan Q, Xiao R, Afolabi M, Bomma M, Xiao Z. Evaluation of Antibacterial Activity of Selenium Nanoparticles against Food-Borne Pathogens. Microorganisms. 2023;11(6):1519.
43. Nguyen THD, Vardhanabhuti B, Lin M, Mustapha A. Antibacterial properties of selenium nanoparticles and their toxicity to Caco-2 cells. Food Control. 2017;77:17-24.
44. Geoffrion LD, Hesabizadeh T, Medina-Cruz D, Kusper M, Taylor P, Vernet-Crua A, et al. Naked Selenium Nanoparticles for Antibacterial and Anticancer Treatments. ACS Omega. 2020;5(6):2660-2669.
45. Nastulyavichus A, Kudryashov S, Smirnov N, Saraeva I, Rudenko A, Tolordava E, et al. Antibacterial coatings of Se and Si nanoparticles. Appl Surf Sci. 2019;469:220-225.
46. Lian S, Fan S, Yang Y, Yu B, Dai C, Qu Y. Selenium nanoparticles

with photocatalytic properties synthesized by residual activated sludge. Sci Total Environ. 2022;809:151163.
47. Fardsadegh B, Jafarizadeh-Malmiri H. Aloe vera leaf extract mediated green synthesis of selenium nanoparticles and assessment of their In vitro antimicrobial activity against spoilage fungi and pathogenic bacteria strains. Green Processing and Synthesis. 2019;8(1):399-407.
48. Cheng H, Wang L, Jia S, Wang L, Cheng S, Lu Y, et al. Green Synthesis of Selenium Nanoparticles by Grape Seed Extract Synergized with Ascorbic Acid: Preparation Optimization, Structural Characterization, and Functional Activity. Foods. 2025;14(17):3002.
49. Soliman MKY, Amin MA-A, Nowwar AI, Hendy MH, Salem SS. Green synthesis of selenium nanoparticles from Cassia javanica flowers extract and their medical and agricultural applications. Sci Rep. 2024;14(1).
50. Ramamurthy CH, Sampath KS, Arunkumar P, Kumar MS, Sujatha V, Premkumar K, et al. Green synthesis and characterization of selenium nanoparticles and its augmented cytotoxicity with doxorubicin on cancer cells. Bioprocess and Biosystems Engineering. 2013;36(8):1131-1139.
51. Khan MA, Singh D, Arif A, Sodhi KK, Singh DK, Islam SN, et al. Protective effect of green synthesized Selenium Nanoparticles against Doxorubicin induced multiple adverse effects in Swiss albino mice. Life Sci. 2022;305:120792.
52. Olaoye AB, Owoeye SS, Nwobegu JS. Facile green synthesis of plant-mediated selenium nanoparticles (SeNPs) using Moringa oleifera leaf and bark extract for targeting α-amylase and α-glucosidase enzymes in diabetes management. Hybrid Advances. 2024;7:100281.
53. Piacenza E, Presentato A, Ferrante F, Cavallaro G, Alduina R, Chillura Martino DF. Biogenic Selenium Nanoparticles: A Fine Characterization to Unveil Their Thermodynamic Stability. Nanomaterials. 2021;11(5):1195.
54. Ramachandran T, Manoharan D, Natesan S, Rajaram SK, Karuppiah P, Shaik MR, et al. Synthesis and Structural Characterization of Selenium Nanoparticles–Bacillus sp. MKUST-01 Exopolysaccharide (SeNPs–EPS) Conjugate for Biomedical Applications. Biomedicines. 2023;11(9):2520.
55. Qiu W-Y, Wang Y-Y, Wang M, Yan J-K. Construction, stability, and enhanced antioxidant activity of pectin-decorated selenium nanoparticles. Colloids Surf B Biointerfaces. 2018;170:692-700.
56. Srivastava N, Mukhopadhyay M. Biosynthesis and structural characterization of selenium nanoparticles mediated by Zooglea ramigera. Powder Technol. 2013;244:26-29.
57. Shitu IG, Katibi KK, Taura LS, Muhammad A, Chiromawa IM, Adamu SB, et al. X-ray diffraction (XRD) profile analysis and optical properties of Klockmannite copper selenide nanoparticles synthesized via microwave assisted technique. Ceram Int. 2023;49(8):12309-12326.
58. Chrissafis K, Roumeli E, Paraskevopoulos KM, Nianias N, Bikiaris DN. Effect of different nanoparticles on thermal decomposition of poly(propylene sebacate)/ nanocomposites: Evaluation of mechanisms using TGA and TG–FTIR–GC/MS. J Anal Appl Pyrolysis. 2012;96:92-99.
59. Alghunaim NS. Characterization of selenium oxide nanofiller effect on the spectroscopic and thermal properties of Cs/ PAM nanocomposites. Journal of Materials Research and Technology. 2020;9(3):3502-3510.
60. El-Behery RR, El-Sayed E-SR, El-Sayyad GS. Gamma rays-assisted bacterial synthesis of bimetallic silver-selenium nanoparticles: powerful antimicrobial, antibiofilm, antioxidant, and photocatalytic activities. BMC Microbiol. 2023;23(1).
61. Ahmad W, Shams S, Ahmad A, Wei Y, Yuan Q, Khan AU, et al. Synthesis of selenium–silver nanostructures with enhanced antibacterial, photocatalytic and antioxidant activities. Applied Nanoscience. 2019;10(4):1191-1204.
62. Ozdal OG. Green synthesis of Ag, Se, and Ag2Se nanoparticles by Pseudomonas aeruginosa: characterization and their biological and photocatalytic applications. Folia Microbiologica. 2023;69(3):625-638.
63. Indhira D, Aruna A, Manikandan K, Albeshr MF, Alrefaei AF, Vinayagam R, et al. Antimicrobial and Photocatalytic Activities of Selenium Nanoparticles Synthesized from Elaeagnus indica Leaf Extract. Processes. 2023;11(4):1107.
64. Dutta RK, Nenavathu BP, Talukdar S. Anomalous antibacterial activity and dye degradation by selenium doped ZnO nanoparticles. Colloids Surf B Biointerfaces. 2014;114:218-224.